1-1-1988

Limits on »raquo;e oscillations

L. S. Durkin
The Ohio State University

R. W. Harper
The Ohio State University

T. Y. Ling
The Ohio State University

J. W. Mitchell
The Ohio State University

T. A. Romanowski
The Ohio State University

See next page for additional authors

Limits on $\bar{\nu}_\mu \rightarrow \bar{\nu}_e$ Oscillations

L. S. Durkin, R. W. Harper, T. Y. Ling, J. W. Mitchell, T. A. Romanowski, E. S. Smith, and M. Timko[a]
The Ohio State University, Columbus, Ohio 43210

S. J. Freedman and J. Napolitano
Argonne National Laboratory, Argonne, Illinois 60439

B. K. Fujikawa and R. McKeown
California Institute of Technology, Pasadena, California 91125

K. T. Lesko
Lawrence Berkeley Laboratory, Berkeley, California 94720

W. C. Choi,[b] A. Fazely, R. L. Imlay, and W. J. Metcalf
Louisiana State University, Baton Rouge, Louisiana 70803

R. D. Carlini,[c] J. B. Donahue, G. T. Garvey, and V. D. Sandberg
Los Alamos National Laboratory, Los Alamos, New Mexico 87545
(Received 18 July 1988)

The result of a search for the neutrino oscillation mode $\bar{\nu}_\mu \rightarrow \bar{\nu}_e$ in a fine-grained tracking detector is reported. The average neutrino energy is 40 MeV and the average detector distance from the neutrino source is 26.8 m. No evidence for neutrino oscillations through this mode is observed. Limits on δm^2 and $\sin^2(2\theta)$ are presented.

PACS numbers: 12.15.Ff, 14.60.Gh

The phenomenon of neutrino oscillations[1] has been actively searched for in recent years.[2] Neutrinos of a given type may oscillate into another if one or more of the neutrino types are massive and if the conservation of lepton family number is violated. With the assumption of two types of neutrinos, the probability of an initial neutrino ν_α of energy E (in MeV) oscillating into a neutrino ν_β after a path length L (in meters) is given by

$$P(\nu_\alpha \rightarrow \nu_\beta) = \sin^2(2\theta)\sin^2(1.27\delta m^2 L/E)\,, \qquad (1)$$

where δm^2 (in eV^2) is the difference of the squares of the masses of neutrino mass eigenstates and θ is the mixing angle between them. In this Letter we report the results of an experiment designed to search for the appearance of $\bar{\nu}_e$ resulting from the oscillation mode $\bar{\nu}_\mu \rightarrow \bar{\nu}_e$.

The experiment is carried out at the Los Alamos Meson Physics Facility (LAMPF experiment No. E645). The neutrino source consists of an equal admixture of ν_μ, $\bar{\nu}_\mu$, and ν_e arising from decays of stopping π^+ and μ^+ produced by 780-MeV protons in a beam stop.[3] The neutrinos are produced isotropically in the energy range 0–52.8 MeV. The $\bar{\nu}_e$ arising from $\bar{\nu}_\mu \rightarrow \bar{\nu}_e$ oscillations will be detected by the inverse-β-decay reaction

$$\bar{\nu}_e + p \rightarrow e^+ + n\,. \qquad (2)$$

The neutrino detector,[4] located 26.8 m from the beam stop, is constructed of 40 liquid-scintillator planes and 41 x-y pairs of proportional-drift-tube (PDT) planes (Fig. 1). A liquid-scintillator plane consists of twelve cells, each 30 cm high by 366 cm long by 3 cm thick in the beam direction, viewed by a photomultiplier tube (PMT) at each end. A plane of PDT has 45 cells, each 7.6 cm × 366 cm × 3.8 cm in dimension. Thin layers of gadolinium deposited on Mylar sheets are placed between the scintillator and PDT planes for the detection of neutrons from reaction (2). The detector has a total mass of 20 metric tons.

Discrimination against cosmic rays is provided by an

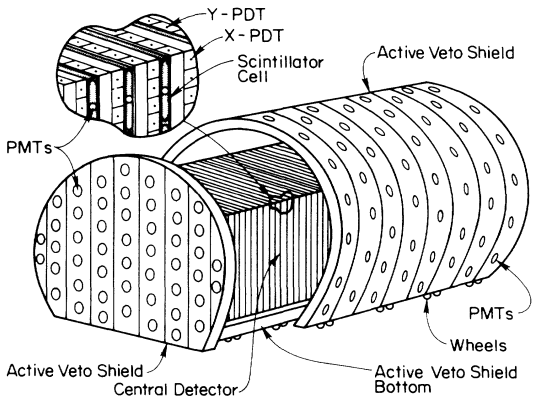

FIG. 1. Isometric view of the detector and the cosmic-ray veto shield.

active 4π shield,[5] also shown in Fig. 1. The close-ended cylinder is 7.6 m in diameter and consists of two layers: a 15-cm-thick outer layer of liquid scintillator viewed by a total of 360 PMT and an inner layer made of 13 cm of lead and 5 cm of iron. During data taking, both the detector and the active shield are placed in a tunnel covered with a minimum of 2000-g/cm^2 overburden of steel to eliminate the hadronic component of the cosmic-ray flux onto the detector.

In the data-taking mode, the detector is triggered by the coincidence of cells in three out of four contiguous scintillation planes and vetoed by hits in the active shield up to 10 μs earlier. Triggers are accepted during 780-μs-long beam spills and during a cosmic-ray gate about 3 times longer in duration. The instantaneous trigger rate is 0.53 Hz in both gates. The average dead time of the experiment is $\sim 16\%$.

The readout electronics is designed to record the activity in the detector and the active shield from 53 μs before the trigger to 107 μs after the trigger. Pulses from the PMT and PDT wires in this time window are stretched and digitized by flash analog-to-digital convertors, stored in memory chips and read out after each trigger. The information after the trigger is used to tag neutrons from reaction (2) which have thermalized and captured on Gd. The time history is used in the off-line analysis to reject muons which have entered the detector 10 μs prior to the trigger.

The results presented here are obtained during LAMPF running cycles over a six-month period. A total of 5100 C of protons are incident on the beam stop during the live time of the experiment, yielding 3.14×10^{13} ν's/cm^2 at the detector.[6] The majority of the 1.27×10^6 triggers written onto tapes are cosmic-ray induced and fall into one of the three categories: electrons from stopping-muon decays, through-going muons, and low-energy nontrackable debris. These raw triggers are subjected to a software filter which requires that (i) there are no digitized hits in the shield within ± 0.5 μs of the trigger time, (ii) a track could be reconstructed for the event, (iii) the event is contained within the fiducial volume of the detector, and (iv) the event is not due to a stopped-muon decay. The stopped-muon events are signified by the spatial coincidence between the triggering particle and an incoming muon up to 20 μs prior to the trigger. These events provide a clean sample of electrons in the same energy range as the positron from reaction (2). They are saved as a control sample for measuring the analysis efficiency and for calibrating the energy response of the detector. Roughly 3% of the events remain after these simple cuts.

The fine granularity of the detector is very well suited for identifying electrons in the 10–100-MeV energy range, as demonstrated in Fig. 2. The likelihood of a track being an electron is calculated based on the differential energy depositions in the liquid-scintillator

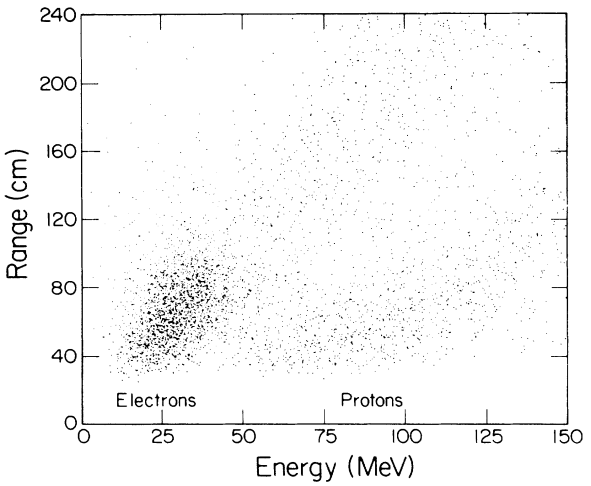

FIG. 2. Scatter plot of visible energy vs range of contained tracks. The dense cluster at the lower left corner of the plot are electrons from stopped-muon decays.

cells and the PDT cells traversed. Protons in the data sample are removed with a rejection factor better than 10^{-3} by requiring that the track must pass as an electron in the likelihood analysis and that the energy deposition in the scintillator cells at either end of the track must be less than 1.5 times minimum ionizing. Electron-like events induced by neutrons are eliminated by a cut on the in-time energy deposition in cells separated from the track. Finally the events in the remaining data sample are required to have no hits in the shield from -30 μs to the trigger time to remove any remaining background from stopping muons.

The contained electron or positron events which pass the above mentioned cuts are candidates for neutrino interactions. In the energy range 0–60 MeV there are 20 events in the beam-on gate [total live time of 76.4 live days (LD's)] and 27 events in the beam-off gate (total live time of 269.2 LD's), where 1 LD is equal to 6.4% (LAMPF duty cycle) of a day, or 5529.6 s. After subtracting the beam-off (cosmic-ray) background of 0.10 ± 0.02 events/LD, we obtain a beam excess of 12.3 ± 4.7 events.

The efficiency for keeping contained electron events due to cuts employed in the analysis is measured to be 0.42 ± 0.03 with electrons from stopping-muon decays. The energy response of the detector is also monitored and calibrated with stopped-muon events. Figure 3(a) shows the measured visible energy distribution for electrons from stopping-muon decays. The agreement with Monte Carlo[7] prediction is excellent.

There are four possible sources of the beam excess events: (i) beam associated neutrons; (ii) charged-current (CC) interactions of ν_μ or $\bar{\nu}_\mu$ from decay in flight (DIF) of pions produced upstream of the beam stop; (iii) background interactions of neutrinos produced at the

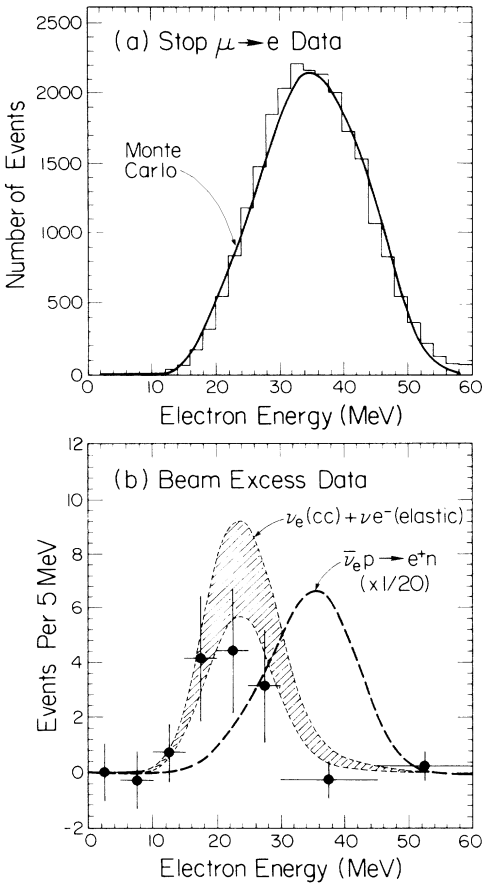

FIG. 3. (a) Visible-energy distribution of electrons from stopped-muon decays. The curve is the Monte Carlo prediction. (b) Visible-energy distribution for the beam-excess electrons. The crosshatched curve is the expected electron spectrum for ν_e CC reactions and νe elastic reactions. The dashed curve shows the maximum oscillation signal, i.e., the positron spectrum from inverse-β reaction (2), scaled down by a factor of 20.

beam stop; and (iv) neutrino oscillation, i.e., positrons from reaction (2).

We can empirically rule out the first two possibilities. The incident neutron flux is monitored by the detected rate of contained knock-on proton events. The measured beam-excess rate of less than 1.4 protons/LD gives an upper limit of 18 beam-neutrons incident on the detector per LD, far too small to account for the beam-excess electron events.[8] The DIF ν_μ (or $\bar{\nu}_\mu$) interactions will produce muons which stop and decay into e^- (or e^+), contaminating the data if the decaying muons have sufficiently low visible energies. Monte Carlo calculations show that for every identified muon due to DIF sources there should be 0.16 ± 0.09 for which the muon energy is too low for it to be visible. We search for contained μ-e events and find 11.5 beam-excess candidates which translate into only 1.8 ± 1.0 DIF background events.

We next examine the possibility that the observed beam-excess events are due to conventional background from the dominant neutrinos—CC interactions of ν_e on various nuclei in the detector (^{12}C, ^{13}C, ^{27}Al, ^{16}O) and elastic neutrino- ($\nu_e, \nu_\mu, \bar{\nu}_\mu$) electron scatterings. The cross sections and the predicted number of events for each of the background reactions and for reaction (2) are listed in Table I. The energy distribution of the beam-excess events is shown in Fig. 3(b). The data are found to be consistent with the shape and the normalization of the predicted spectrum of ν_e CC and νe^- elastic reactions, shown as the shaded band which represent the systematic error of the prediction (15% in neutrino flux and 20% in cross sections[9,10]). Also shown in Fig. 3(b) is the energy spectrum for the inverse-β-decay reaction (2), assuming maximum oscillation (dashed curve). The signal for neutrino oscillation is expected to peak at substantially higher energy than the data. *We therefore conclude that the beam-excess events are well explained by background neutrino interactions and there is no evidence for neutrino oscillations through the mode* $\bar{\nu}_\mu \rightarrow \bar{\nu}_e$.

We have analyzed the beam-excess events for the presence of delayed neutrons which would accompany positrons from reaction (2). Such neutrons are captured in the gadolinium planes and detected by subsequent interaction of the capture γ rays in the scintillator. The efficiency for detection of these neutrons is 20.1%, based

TABLE I. Expected number of events from ν_e and $\bar{\nu}_e$ interactions for a total neutrino flux of $3.14\times10^{13}/\text{cm}^2$ incident on the detector. The number of events for the $\bar{\nu}_e p \rightarrow e^+ n$ reaction is for maximum oscillation, i.e., $P(\bar{\nu}_\mu \rightarrow \bar{\nu}_e) = 1$.

Reaction	Cross section (cm^2)	No. of Target nuclei	Trigger acceptance	Calculated No. events
$\bar{\nu}_e p \rightarrow e^+ n$	1.02×10^{-40}	1.05×10^{30}	0.333	470.3 ± 75
$\nu_e\,^{12}\text{C} \rightarrow e^-\,^{12}\text{N}$	1.46×10^{-41}	6.13×10^{29}	0.121	14.3 ± 3.6
$\nu e^- \rightarrow \nu e^-$	4.0×10^{-43}	5.57×10^{30}	0.212	6.2 ± 1.2
$\nu_e\,^{13}\text{C} \rightarrow e^-\,^{13}\text{N}$	4.0×10^{-41}	6.25×10^{27}	0.263	0.9 ± 0.5
$\nu_e\,^{16}\text{O} \rightarrow e^-\,^{16}\text{F}$	5.2×10^{-42}	1.10×10^{29}	0.080	0.6 ± 0.2
$\nu_e\,^{27}\text{Al} \rightarrow e^-\,^{27}\text{Si}$	4.0×10^{-41}	4.63×10^{27}	0.194	0.5 ± 0.3

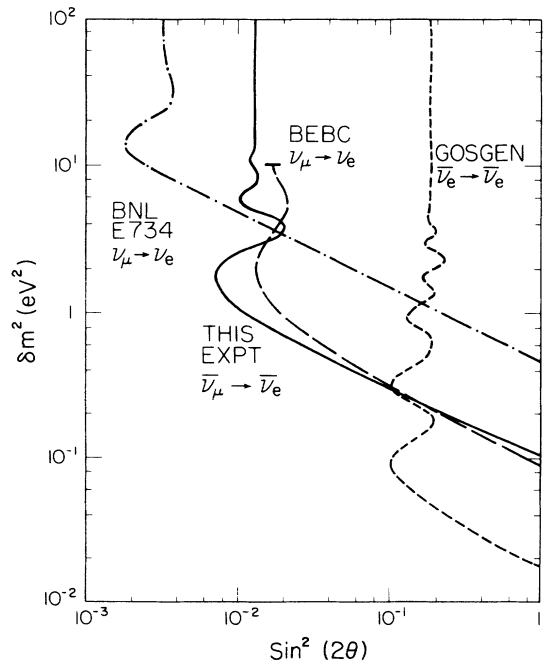

FIG. 4. The 90%-confidence-level contour for the region of δm^2 and $\sin^2(2\theta)$ excluded by this experiment. Other recently published limits (Ref. 2) are shown for comparison.

on Monte Carlo simulations and verified by the use of a tagged fission source placed in the detector. No evidence for the presence of neutrons in coincidence with any of the neutrino candidates is found, consistent with the above conclusion.

We have performed a binned maximum likelihood analysis on the data shown in Fig. 3(b). Limits on δm^2 and $\sin^2(2\theta)$ are established by the use of Eq. (1) and the calculated rate and energy spectrum of the inverse-β reaction[11] and those of the neutrino background reactions. We obtain, at 90% confidence level,

$$\delta m^2 < 0.11 \text{ eV}^2 \text{ for maximal mixing;}$$

$$\sin^2(2\theta) < 0.014 \text{ for large } \delta m^2.$$

Figure 4 gives the 90%-confidence contour for the region excluded by this experiment. Other published limits from previous searches[2] are also shown for comparison.

We are grateful to the administrative and technical staff members of LAMPF for their support during this experiment. We wish to thank the contributions of L. Hyman and B. Musgrave during the early phase of this experiment and the technical assistances of C. J. Rush, J. W. Heimaster, V. K. Sehgal, J. S. Fitch, and M. Anderson of The Ohio State University; J. Dawson, R. Haberichter, and J. Nelson of the Argonne National Laboratory; W. Marterer and J. Ui of Louisiana State University; and N. Thompson of LAMPF. This work has been supported through funds provided by the U.S. Department of Energy.

[a]Present address: Department of Physics, Texas A&M University, College Station, TX 77843.

[b]Present address: Nuclear Science Centre, University of Alberta, Edmonton, Alta. T6G 2J1, Canada.

[c]Present address: Continuous Electron Beam Accelerator Facility, Newport News, VA 23606.

[1]B. Pontecorvo, Zh. Eksp. Teor. Fiz. **33**, 549 (1957) [Sov. Phys. JETP **6**, 429 (1958)], and **53**, 1717 (1967) [**26**, 984 (1968)]; Z. Maki *et al.*, Prog. Theor. Phys. **28**, 870 (1962); S. M. Bilenky and B. Pontecorvo, Phys. Rep. **41C**, 225 (1978).

[2]G. N. Taylor *et al.*, Phys. Rev. D **28**, 2705 (1983); A. F. Bergsma *et al.*, Phys. Lett. **142B**, 103 (1984); J. F. Cavaignac *et al.*, Phys. Lett. **148B**, 387 (1984); L. A. Ahrens *et al.*, Phys. Rev. D **31**, 2732 (1985); V. Zacek *et al.*, Phys. Lett. **164B**, 193 (1985); C. Angelini *et al.*, Phys. Lett. B **179**, 307 (1986).

[3]The π^-'s are mostly absorbed in the beam stop before they decay. The contamination of wrong-sign neutrinos from π^- decays is calculated to be 1.8×10^{-4}.

[4]J. Fitch *et al.*, Nucl. Instrum. Methods Phys. Res. **226**, 373 (1984); L. S. Durkin *et al.*, to be published.

[5]S. J. Freedman *et al.*, Nucl. Instrum. Methods **215**, 71 (1983); J. Napolitano *et al.*, to be published.

[6]Neutrino flux quoted here is calculated with the number of 0.089 ± 0.011 π^+'s produced per incident proton which stopped in the beam stop; see R. C. Allen *et al.*, Phys. Rev. Lett. **55**, 2401 (1975).

[7]The Monte Carlo program used for the calculation contains the EGS4 code and the detector geometry and composition; see W. R. Nelson *et al.*, SLAC Report No. 265, 1985 (unpublished).

[8]The rate of energetic photons (>20 MeV) produced by inelastic neutron reactions is measured to be less than 10^{-3} per incident neutron; S. J. Seestrom-Morris, private communication.

[9]T. W. Donnelly *et al.*, Phys. Lett. **34B**, 93 (1973).

[10]B. Kaiser *et al.*, Phys. Rev. D **20**, 87 (1979).

[11]J. S. O'Connell, LAMPF Report No. LA-9858-C, 1981 (unpublished), p. 43; P. Vogel, Phys. Rev. D **29**, 1918 (1984); S. A. Fayans, Yad. Fiz. **42**, 929 (1985) [Sov. J. Nucl. Phys. **42**, 590 (1986)].

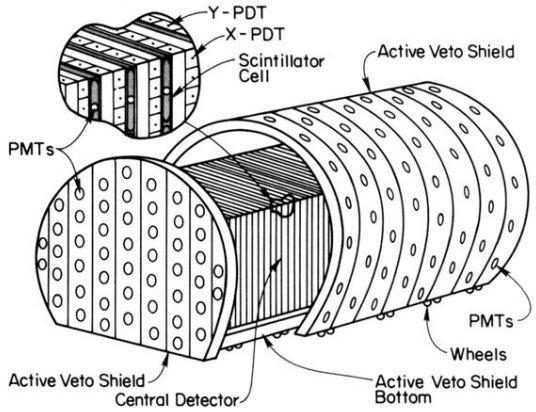

FIG. 1. Isometric view of the detector and the cosmic-ray veto shield.